Far-infrared second-harmonic generation in GaAs/$Al_xGa_{1-x}As$ heterostructures: Perturbative and nonperturbative response

W. W. Bewley, C. L. Felix, J. J. Plombon, and M. S. Sherwin
Department of Physics and Center for Free-Electron Laser Studies, University of California–Santa Barbara, Santa Barbara, California 93106

M. Sundaram, P. F. Hopkins, and A. C. Gossard
Department of Materials, University of California–Santa Barbara, Santa Barbara, California 93106
(Received 11 January 1993)

We report measurements of far-infrared (FIR) harmonic generation from GaAs/$Al_xGa_{1-x}As$ heterostructures. The samples studied were a modulation-doped $Al_{0.3}Ga_{0.7}As$/GaAs heterojunction and a sample with ten modulation-doped half-parabolic quantum wells. The samples were driven with intense far-infrared radiation from a molecular gas laser at 29.5 cm^{-1} and the University of California–Santa Barbara free-electron laser at 51.3 cm^{-1}. The FIR radiation was polarized parallel to the growth direction. Second harmonics of the FIR were detected from both the semi-insulating GaAs substrate and from the confined electrons. For the heterojunction sample, the second-harmonic power generated by the electrons depended quadratically on fundamental power at low power, as expected from time-dependent perturbation theory. However, this dependence became subquadratic at higher powers, indicating a nonperturbative response. At high FIR powers, electrons were also ionized from the heterojunction and half-parabolic wells. For the heterojunction at $f=29.5$ cm^{-1} in the perturbative regime, the surface second-order susceptibility was computed to be $\chi_S^{(2)}=1.0\pm0.75\times10^{-8}$ $esu^{-1}\,cm^3$. This value agrees, within experimental error, with a simple model of the heterojunction as a triangular quantum well. The second-order polarizability of a conduction electron in the heterojunction is nine orders of magnitude larger than that of a valence electron in pure GaAs.

I. INTRODUCTION

The growth of semiconductor heterostructures by molecular-beam epitaxy (MBE) provides the ability to fabricate materials with enhanced nonlinear optical properties by "band-gap engineering."[1] Early predictions of enhanced second-order optical nonlinearity of electrons in asymmetric quantum wells were made by Gurnick and DeTemple.[2] In quantum wells pumped by mid-infrared (mid-IR) radiation ($\lambda\approx10$ μm) second-[3–7] and third-order[8] nonlinear susceptibilities several orders of magnitude larger than bulk GaAs have been reported, in good agreement with theoretical predictions. Experiments and calculations on the nonlinear response of electrons in heterostructures will improve understanding of the interaction of intense radiation with many-electron systems, and may lead to important applications such as mixers, frequency multipliers, and parametric amplifiers.

The origin of the enhanced nonlinear susceptibility in quantum wells can be understood by examining the form of the nth-order nonlinear polarizability of an electron, which is calculated in nth-order perturbation theory. The nonlinear polarizability $\alpha^{(n)}$ is a sum of terms, each of which is of the form[9,10]

$$\frac{C\prod_{1}^{n+1}\langle z\rangle_n}{\prod_{1}^{n}(\omega-\Omega_n-i\gamma_n)}. \tag{1}$$

Here, C is a constant, $\langle z\rangle$ is a dipole matrix element, ω is the driving frequency, Ω is an intersubband transition frequency, and γ is a damping rate. The enhancement of the nonlinear susceptibility in quantum wells over the value for bulk GaAs is a result of the large $\langle z\rangle$ and small Ω in quantum wells. Whereas dipole matrix elements for interband transition are of the order of ea, where e is the electric charge and a is the lattice constant (≈5 Å), dipole matrix elements for intersubband transitions can be of the order of eL, where L is the width of the quantum well, which may be hundreds of angstroms. Whereas nonresonant energy denominators associated with interband transitions are of the order of the band gap (1.5 eV), energy denominators for intersubband transitions can be as small as a few meV. Based on these simple arguments, one concludes that the nonlinear susceptibility for $\omega\leq\Omega$ increases dramatically as quantum wells are made wider, and pump wavelengths are extended beyond the mid-IR (10 μm). The ability to grow wide quantum wells with almost arbitrary shapes[11] enables one to design a quantum well to maximize its nonlinear response.

In this paper, we report experimental measurements on harmonic generation in semiconductor heterostructures pumped by far-infrared (FIR) radiation. We have used pumped wavelengths between 200 and 300 μm, generated by a molecular gas laser and the University of California–Santa Barbara (UCSB) free-electron laser. The samples studied contained ten half-parabolic quantum wells and an $Al_{0.3}Ga_{0.7}As$ heterojunction. In a

0163-1829/93/48(4)/2376(15)/$06.00

heterojunction, electrons are confined by an approximately triangular potential.[12] The samples were placed in a strip line coupler with the FIR electric field oriented in the growth direction z. Our principal results are as follows.

(1) Second harmonics (SH) generated by the bulk GaAs substrate were measured in both samples.

(2) Second harmonics generated by the confined electrons were measured in both samples, and clearly distinguished from the second harmonics generated by the bulk.

(3) The intensity of the bulk second harmonic depends quadratically on the intensity of the fundamental, as expected from perturbation theory.

(4) In the heterojunction, the intensity of the second harmonic from the electrons depends quadratically on the intensity of the fundamental at the lowest intensities, but becomes markedly subquadratic at higher intensities.

(5) The quantum wells in both samples could be persistently ionized by intense far-infrared radiation at low temperatures.

(6) A surface nonlinear susceptibility $\chi_S^{(2)}$ was calculated from the data. For the heterojunction at low intensities (where there is a quadratic dependence of the second harmonic on fundamental intensity), $\chi_S^{(2)}=1\pm0.75\times10^{-8}$ $\mathrm{cm^3\,esu^{-1}}$ for $\lambda_{\mathrm{pump}}=339$ μm. This nonresonant $\chi_S^{(2)}$ is larger than the resonance-enhanced $\chi_S^{(2)}$ previously reported in asymmetric wells for $\lambda_{\mathrm{pump}}=10$ μm.[3,4]

(7) A simple calculation of $\chi_S^{(2)}$, modeling the heterojunction as a collection of noninteracting electrons in a triangular potential,[12] predicts $\chi_S^{(2)}=8\times10^{-9}\mathrm{cm^3\,esu^{-1}}$, within experimental error of the measured value. In this triangular well model, the lowest intersubband transition is expected at 290 $\mathrm{cm^{-1}}$, ten times our fundamental frequency.

(8) At the highest intensities, FIR electric fields at the sample have amplitudes of order 20 kV/cm comparable to the internal fields confining electrons at the heterojunction. In order to model the ionization and subquadratic intensity dependence of the second harmonic, perturbation theory must be abandoned and fundamentally new approaches are needed. Previous studies of harmonic generation and ionization from atoms in intense laser fields[13,14] provide a starting point for modeling our results at high intensity.

The rest of the paper is organized as follows. Section II describes samples and experimental techniques. Section III describes experimental results. Section IV describes the analysis of the perturbative experimental results and the extraction of a surface susceptibility $\chi_S^{(2)}$ from the data. Section V compares the perturbative results for the heterojunction with the triangular well model, and discusses qualitatively the nonperturbative response. Finally, Sec. VI concludes the paper. The Appendix A describes the analysis of the electrodynamics of the strip line coupler.

II. SAMPLES AND EXPERIMENTAL TECHNIQUES

A. Samples

The two samples for the experiments were grown by MBE. The substrates were grown (elsewhere) using the liquid-encapsulated Czochralski method, with surface normal along the (100) direction, and were not intentionally doped. Sample 1, shown in Fig. 1(a), was a multiple

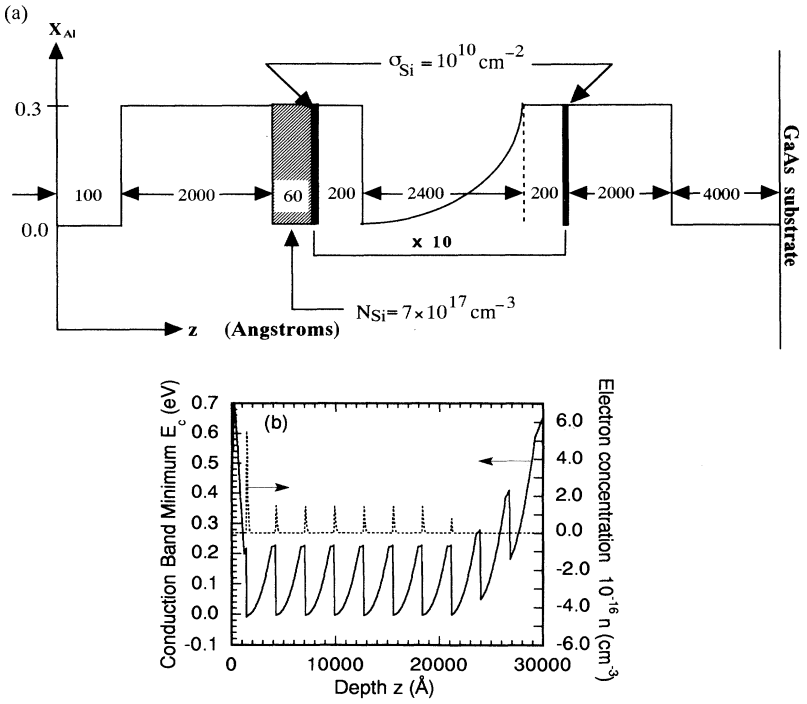

FIG. 1. Half-parabolic-well sample. (a) Compositional profile. The sample contained ten half-parabolic wells. The barrier between each well and its neighbor contains a sheet with an areal density of 2×10^{10} $\mathrm{cm^{-2}}$ Si dopants. (b) Conduction-band diagram and charge density.

quantum-well structure consisting of ten half-parabolic wells (HPW's). Each 2400-Å-wide HPW was grown using a 20-Å-period digital alloy,[15] and was modulation doped.[1] The wells were designed to have a half-parabolic shape, when unoccupied by electrons, and an intersubband spacing of 50 cm^{-1}. The areal electron density was designed to be $N_S = 2\times10^{10}$ cm^{-2} per well assuming 100% ionization of the donors, which would correspond to a partially occupied ground state for the well. Figure 1(b) shows the conduction-band minimum and charge density calculated for this structure by solving the Schrödinger and Poisson equations self-consistently at zero temperature.[16] This simulation predicts, for the first well (closest to surface), $N_S = 7\times10^{10}$ cm^{-2}, for wells 2–7 $N_S = 2\times10^{10}$ cm^{-2}, for well 8 $N_S = 0.6\times10^{10}$ cm^{-2}, and wells 9 and 10 empty.

Sample 2 was a standard $Al_{0.3}Ga_{0.7}As/GaAs$ heterojunction, shown in Fig. 2(a). The physics of heterojunctions is described in detail in Refs. 1 and 12. Figure 2(b) shows the conduction-band minimum and electron concentration for the heterojunction, again determined from a self-consistent solution of the Schrödinger and Poisson equations. The predicted sheet density for this sample is $N_S = 3.4\times10^{11}$ cm^{-2}. Stern and Das Sarma[12] estimate the ground-to-first-excited-state transition to be greater than 160 cm^{-1} for a heterojunction doped at $N_S = 5\times10^{11}$ cm^{-2}, the measured areal density for our sample.

1. *Sample characterization*

The samples were electrically characterized by standard Hall and Shubnikov–de Haas measurements. The samples were dark cooled (i.e., cooled while shielded from room light) to $T = 4.2$ K and then illuminated with a light-emitting diode (LED). The purpose of illuminating the sample with the LED is to use the persistent photoconductivity effect associated with deep donors in $Al_xGa_{1-x}As$ to persistently ionize the donors that may trap electrons upon cooling.[17] These deep donors are called *DX* centers. The results for the carrier density and mobility are shown in Table I.

TABLE I. Carrier concentration and mobility for investigated samples. All values are quoted for cooling the sample below 10 K in the dark, then illuminating with an IR LED. Carrier concentration and mobility were determined from mangetotransport measurements.

Sample	Sheet density (cm^{-1})	Mobility (cm^2/V sec)	Carriers on dark-cool
Heterojunction	5×10^{11}	4.4×10^5	yes
Half-parabolic	5.6×10^{11}	2×10^5	no

The carrier density for the 10-HPW sample is the total carrier density for all ten wells. This value of $N_S = 5.6\times10^{11}$ cm^{-2} is a factor of 2 greater than the designed total density of $N_S = 2\times10^{11}$ cm^{-2} and indicates that some of the electrons in the 60-Å-thick, 7×10^{17}-cm^{-3}-doped region near the surface were ionized and transferred into the wells. Capacitance-voltage profiling of a sample from the same wafer as the one on which the optical experiments were performed indicates that the charge was in fact concentrated in thin slabs in the first two wells, with 3.6×10^{11} cm^{-2} in the first well, 1.4×10^{11} cm^{-2} in the second well, and no electrons in the other

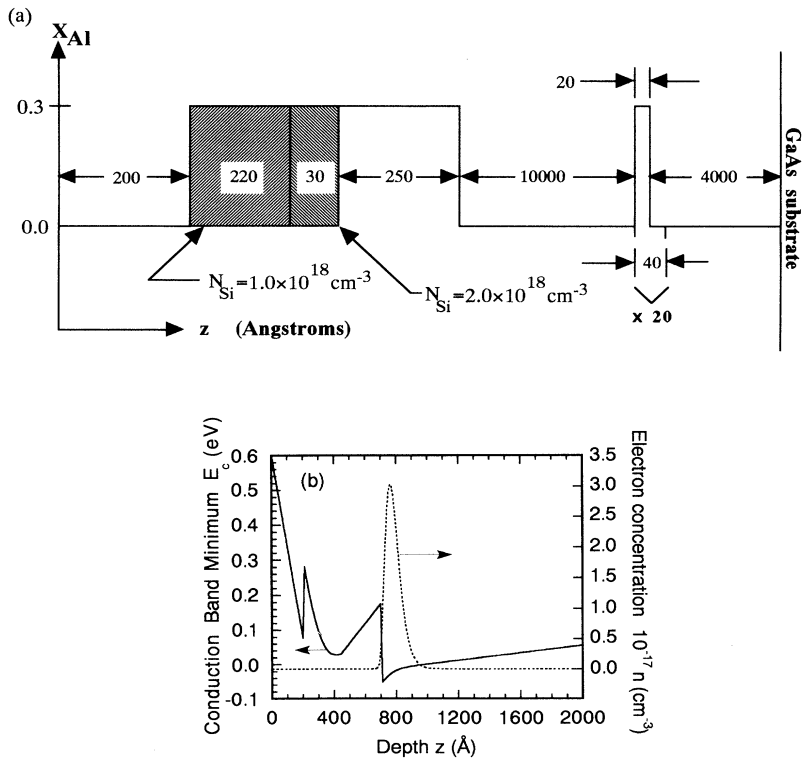

FIG. 2. Heterojunction sample. (a) Compositional profile. (b) Conduction-band diagram and charge density.

wells. At these large sheet densities, Coulomb effects dominate the potential built in by grading the conduction band, and the potential felt by an electron resembles that at a heterojunction. When cooled in the dark, the HPW sample was nonconducting. After cooling, it was necessary to illuminate it with a LED to populate it with carriers.

2. *Sample configuration for second-harmonic experiments*

The samples were cleaved to the dimensions given in the caption to Fig. 3. To allow monitoring and control of the electron density in the sample during optical experiments, the sample was patterned with a gate (1000 Å of Au on Ti) and two Au/Ge/Ni/Au Ohmic contacts (source, drain), as shown in Fig. 3. The contacts were annealed prior to evaporation of the gate.

Electrically, the samples were configured in two ways. In the first configuration the gate was floating while the source and drain were connected across a current source. The above configuration was used to monitor the resistance of the two-dimensional electron gas (channel) and thus approximately track the electron density of the samples. In the second configuration the source and drain were grounded and a negative voltage was applied to the gate to deplete the sample of free carriers.

B. Experimental techniques

1. *FIR sources*

For the experiments two different FIR sources were used. The first was a molecular gas laser (MGL). The MGL consists of a Lumonics TEA-100-2 pulsed CO_2 transverse excited atmospheric (TEA) laser and a 16-ft-long glass tube that is 3.8 cm in diameter. The TEA laser produces pulsed mid-IR radiation and is discretely tuned between 9 and 11 μm by means of a rotatable grating. Mid-IR pulses approximately 60 ns in length were produced with a repetition rate of up to 0.5 Hz. The glass tube was filled with methylfluoride for our experiments and produced FIR radiation when pumped with the mid-IR radiation. Gross *et al.*[18] have tabulated the FIR frequencies for various gases and mid-IR pump lines. The FIR pulses are approximately 60 ns long. Unfortunately, the power fluctuates on a nanosecond time scale within each pulse.[19] The energy contained in a FIR pulse fluctuates by $\approx 50\%$ from pulse to pulse. Most of our experiments with the MGL were performed at a frequency of 29.5 cm^{-1}. The energy per pulse for this line was approximately 5 mJ, corresponding to an average power of approximately 80 kW during the pulse. Given the nanosecond intrapulse time structure, the peak power during a pulse is expected to exceed the average power.

The other FIR source used for the measurements was the UCSB free-electron laser (FEL). For our experiments we tuned the FEL to produce 51.3-cm^{-1} radiation. The FEL produced smooth pulses approximately 2.5 μs in length with an energy of approximately 2.5 mJ per pulse at a repetition rate of 0.3 Hz. The average power was approximately 1 kW during a pulse.

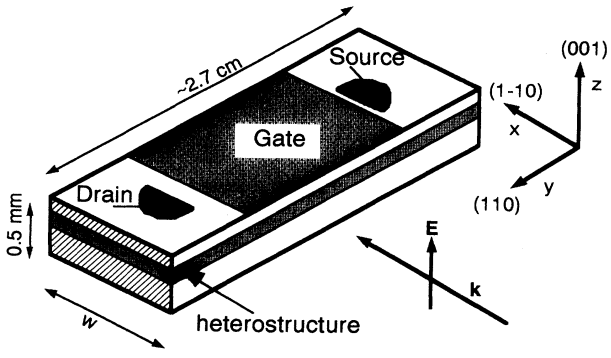

FIG. 3. Sample and contact geometry. For the half-parabolic-well and heterojunction samples, $w = 0.5159 \pm 0.0003$ and 0.4943 ± 0.0003 cm. The width of the gate in the long direction of the sample is approximately 0.5 cm.

2. *Optics*

Optics were laid out to couple the fundamental FIR radiation into the sample and then collect and characterize the generated second harmonics. Characterization of the harmonics involves the determination of the polarization-, frequency-, and intensity-dependence of the generated harmonics with respect to the fundamental. A schematic of the experimental optical layout is shown in Fig. 4.

The fundamental FIR beam was initially incident upon a mylar beam splitter (beam splitter no. 1) that split off about 1% of the radiation, which was then focused onto a

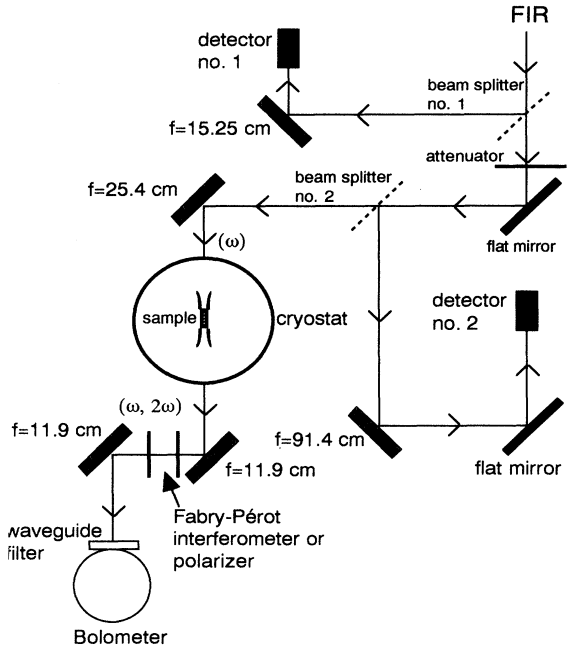

FIG. 4. Schematic diagram of the optical setup used to measure second-harmonic generation from heterostructures.

pyroelectric detector (detector no. 1). The signal generated from this detector was used to trigger the data-acquisition electronics and functions to reject misfired or very-low-power pulses from the MGL. To vary the intensity of the fundamental beam, it was attenuated by polymethyl methacrylate (PMMA) attenuators before beam splitter no. 2 and after beam splitter no. 1. Beam splitter no. 2 split off about 1% of the radiation, which was then focused onto a pyroelectric detector (detector no. 2). The signal generated from this detector provided a reference signal for monitoring the relative energy of the fundamental beam after passing through the attenuators. The incident beam was then focused with a 10-in. focal length 90° off-axis paraboloidal mirror into the strip line coupler/cryostat in which the samples were mounted. A schematic of the strip line coupler is shown in Fig. 5. The beam emitted from the strip line coupler was collimated with a 119-mm focal length 90° off-axis paraboloidal mirror. A scanning Fabry-Pérot interferometer or polarizer could be inserted into the collimated beam and used to determine the frequency content or polarization of the emitted beam. The collimated beam was then focused with another 119-mm focal length mirror onto a waveguide cutoff filter that was mounted on the front of an Infrared Labs model HD-3 Si bolometer operating at $T=4$ K. The waveguide cutoff filter has a cutoff frequency of 58.6 cm^{-1} and the principles of its operation are described in Ref. 20. The purpose of the waveguide cutoff filter was to reject the fundamental beam and pass the second harmonic. At 29.5 cm^{-1}, where most of the measurements reported in this paper were performed, the high-pass filter had no detectable transmittance even when the full power of the MGL was focused onto the filter, indicating a transmittance less than 10^{-11}. The bolometer measured the energy of the beam that passed through the filter. The overall collection efficiency of the filter and bolometer was measured to be approximately 3% at 66 cm^{-1}.

The reference signal generated by detector no. 2 and the bolometer signal were recorded with an EG and G model 4402 signal processor in conjunction with a model 4420 boxcar averager and model 4422 gated integrator modules. The above configuration provides an adjustable gate that was used to select, integrate, and average over a portion of the signals. The signals produced by each laser pulse were recorded separately.

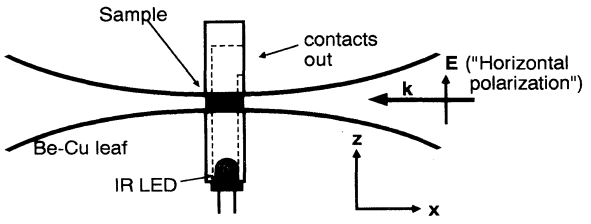

FIG. 5. Schematic diagram of the strip line and horn coupler. The infrared LED (TRW OP290, photon energy 1.42 eV) is used to ionize deep traps and populate the quantum well with electrons.

III. EXPERIMENTAL RESULTS

In this section we will present the results of measurements performed on the 10-HPW and heterojunction samples. The measurements involved coupling the fundamental radiation from either the MGL or FEL into the samples with the previously described optical setup and measuring the radiation emitted from the samples. The emitted radiation was characterized by its spectral content, dependence on the condition of the sample (i.e., electron density), polarization, and intensity dependence.

A. Ionization

In the first experiments on SH generation from the HPW sample, we discovered to our surprise that the intense FIR radiation could persistently ionize the HPW. When cooled in the dark to $T=7$ K, the HPW sample contained a negligibly small carrier concentration, as evidenced by a source-drain resistance exceeding 20 MΩ. On flashing with an IR LED after dark cooling, the resistance dropped to 400 Ω. In Fig. 6, the source-drain resistance is plotted versus time with the IR LED off. Each vertical jump in resistance coincides with a single pulse from the MGL. Successive laser pulses drive the resistance from near 400 Ω to an asymptotic value near 650 Ω, suggesting that a large number of electrons have been depleted from the quantum wells. It is possible that the residual conductivity is through the doped layer which is parallel to the quantum wells—both quantum wells and the doped layers can exhibit persistent photoconductivity when illuminated with a LED. In Fig. 6(b) the source-drain resistance is plotted versus time with the IR LED on. Here, each FIR laser pulse drives the resistance up, but the resistance recovers between each FIR pulse as radiation from the LED repopulates the well with carriers.

We propose a two-step process to explain the results of

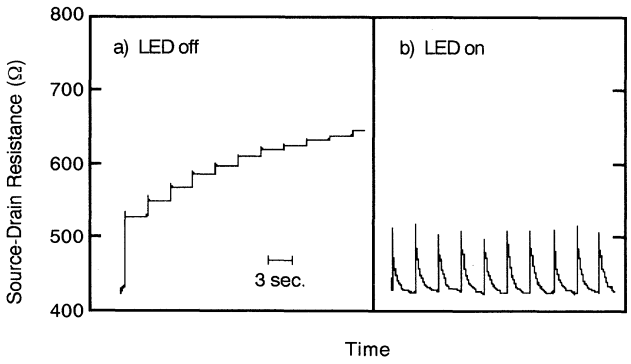

FIG. 6. Ionization of the half-parabolic well by intense FIR radiation. (a) Source-drain resistance R_{SD} vs time with LED off. Each laser pulse causes a persistent jump in R_{SD}, indicating that electrons have been persistently removed from the well. (b) R_{SD} vs time with LED on. The resistance recovers after each laser pulse, as the LED repopulates the quantum well with electrons. The FIR source was the molecular gas laser. FIR pump frequency=43.3 cm^{-1}, FIR pulse length ≈60 ns, pulse energy ≈5 mJ, repetition rate=0.25 Hz, $T\approx 7$ K. Similar behavior occurred for FIR pump frequency=29.5 cm^{-1} and in the heterojunction sample.

Fig. 6.

(1) The FIR radiation first transfers sufficient kinetic energy to ionize the well (i.e., to send the electrons into the doped $Al_{0.3}Ga_{0.7}As$ barriers). For a FIR electric field of 10 kV/cm, the electric-field energy drop across the width of the 2400-Å well is 240 meV, comparable to the depth of the well. Thus ionization appears likely.

(2) The electrons are then captured by *DX* centers. We have proven that the second step can occur in experiments on a sample containing only a Si-doped, 2-μm-thick $Al_{0.3}Ga_{0.7}As$ epilayer, and no quantum well.[21] That sample was cooled in the dark and irradiated with an IR LED to ionize *DX* centers and induce persistent photoconductivity. The sample was then exposed to intense FIR radiation with photon energy of a few meV. The carrier concentration was reduced with each pulse of FIR radiation, indicating that intense FIR radiation can indeed induce capture of electrons by *DX* centers. Possible mechanisms are discussed in Ref. 21.

B. Measurement protocols

In view of the ionization induced by the intense FIR radiation we developed the following standard procedure for conditioning the samples prior to an FIR pulse: the diode was turned on for 1 s in between successive FIR pulses, and turned off approximately 200 ms before each FIR pulse. This procedure consistently restored the source-drain resistance (and hence the electron concentration) to the same level, independent of the FIR intensity. In the rest of this paper, *diode on* means that the diode was turned on between FIR pulses, and *diode off* means that it was not turned on.

The electron concentration in the channel could also be controlled in a more conventional and reproducible fashion by applying a negative gate bias to deplete the electrons from the well. In the rest of the paper, *depleted* means that a negative gate voltage sufficient to deplete the well of electrons was applied, and *full* means that zero gate voltage was applied.

In this section we will first present the results of second-harmonic measurements on the 10-HPW sample using pump frequencies of 29.5 cm^{-1} from the MGL and 51.3 cm^{-1} from the FEL. A third harmonic of 27.7 cm^{-1} was also observed, but is discussed only briefly. We will then present results of second-harmonic measurements on the heterojunction pumped by 29.5-cm^{-1} radiation. For each sample at each pump frequency, three kinds of data are presented.

(1) The frequency of radiation reaching the bolometer is analyzed by scanning a Fabry-Pérot interferometer.

(2) The dependence on the electron concentration of each polarization component of the radiation reaching the bolometer is analyzed by comparing the bolometer signal with diode on and diode off or full and depleted.

(3) The intensity of the second harmonics generated by the electrons and the bulk are plotted as a function of fundamental intensity.

C. Half-parabolic well sample

1. $f = 29.5\ cm^{-1}$, molecular gas laser

The following results are from the 10-HPW sample at $T = 7$ K, with a pump frequency of 29.5 cm^{-1} from the MGL. The bolometer signal produced by the radiation emitted from the sample and transmitted through the Fabry-Pérot interferometer (FPI) is plotted versus the separation of the meshes of the FPI in Fig. 7. Each point plotted is the average of 20 FIR pulses at the separation shown. The uncertainty in the separation is approximately the width of the circles. The data were taken with zero gate voltage, the diode on, and no polarizer or attenuators. The pump frequency of 29.5 cm^{-1} corresponds to a wavelength of 339 μm. The peaks in Fig. 7 are separated by approximately 85 μm and imply that the wavelength of the emitted radiation is 170 μm or the frequency is 59 cm^{-1}, double the pump frequency. The wavelength of the emitted and pump beams was more precisely determined by measuring the FPI mesh separation corresponding to 30 and 50 peaks for the two beams, respectively. The results are shown in Table II. We conclude that all of the radiation being detected by the bolometer is second harmonics emitted by the sample. There is no detectable fundamental leakage. The third harmonic of 29.5 cm^{-1}, were it emitted by the sample, would have been blocked by a water vapor absorption.

A polarizer was inserted after the sample to characterize the polarization of the SH and its dependence on the electron concentration in the quantum wells. In Fig. 8 the bolometer signal produced by the horizontal (parallel to the growth direction z) and vertical components of the SH are shown for the two cases diode on and diode off. Each measurement corresponds to an average of 50 FIR pulses. From Fig. 8 we observed that with the diode off there is no component of the SH parallel to z, while the component perpendicular to z appears to be unaffected by whether the diode is on or off. It is shown in the Appen-

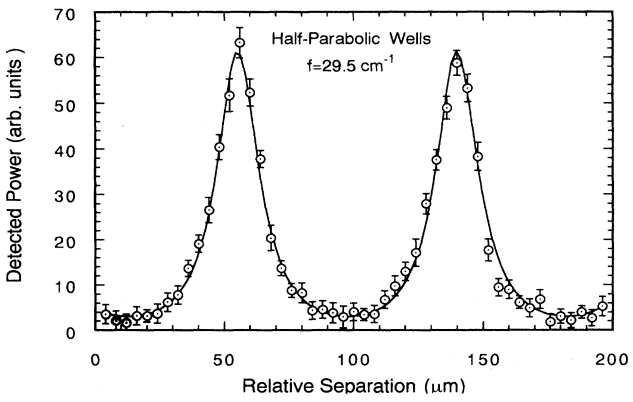

FIG. 7. Fabry-Pérot scan of the signal generated by the HPW sample. The LED was pulsed between each FIR pulse in order to ensure a reproducible population of electrons in the well. The spacing between the peaks is $\lambda/2 = 84.8$ μm, consistent with the second harmonic of the 29.5-cm^{-1} (339-μm) pump radiation from the molecular gas laser. Pulse length ≈ 60 ns, pulse energy ≈ 5 mJ, repetition rate $= 0.25$ Hz, $T \approx 7$ K.

TABLE II. Wavelengths of the fundamental power and power generated in the sample for the molecular gas laser line, showing that the generated power is the second harmonic of the fundamental. Wavelength = Separation/(2×Number) of peaks.

Signal	Number of peaks	Separation (mm)	Wavelength (μm)
Fundamental	50	8.478±0.008	339.12±0.16
Generated	30	2.544±0.008	169.6±0.26

dix that the component of the SH parallel to z is generated from electrons in the well while the component perpendicular to z—the only component present with the diode off—is generated from bulk GaAs.

The dependence of the SH intensity on the pump intensity was measured with the diode on and off. Figure 9(a) plots the second-harmonic power emitted by the sample with the diode off (polarized perpendicular to z), P_{2f}^{off}, versus the fundamental power in the strip line, P_f.[22] Each point is the average of 200 FIR pulses. The experimental data are well fitted by a quadratic with an offset:

$$P_{2f}^{\text{off}}(P_f) = A + B(P_f)^2 . \quad (2)$$

The fitted parameters are $A = 0.144$ μW and $B = 0.61$ W^{-1}. The offset A accounts for a small dc offset voltage in a boxcar integrator.

The intensity dependence of the component of the SH polarized parallel to z (due to the electrons, as we argue below) is shown in Fig. 9(b). Rather than rejecting the component perpendicular to z (due to bulk GaAs) with a somewhat inefficient polarizer, we have extracted the component parallel to z by subtracting the fit (2) to the diode-off signal from the diode-on signal:

$$P_{2f}^{\parallel z} \equiv P_{2f}^{\text{on}} - P_{\text{fit}}^{\text{off}}(P_f) . \quad (3)$$

$P_{\text{fit}}^{\text{off}}$ was computed using the fitted parameters A and B. Each point plotted is from the average of 200 FIR pulses.

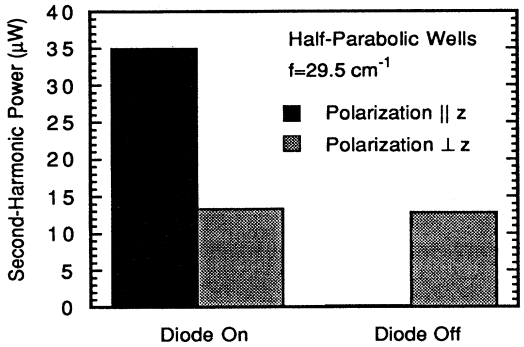

FIG. 8. Polarization content of the signal generated by the half-parabolic-well samples with diode on and diode off. The component parallel to z is reduced by more than 99% with diode off, and is attributed to confined electrons. The component perpendicular to z is unaffected by diode, and is attributed to second harmonics from bulk GaAs.

We see from Fig. 9(b) that the component of the SH$\|z$ does not exhibit a quadratic intensity dependence.

2. $f = 51.3$ cm^{-1}, UCSB FEL

Measurements on the 10-HPW sample with a pump frequency of 51.3 cm^{-1} were performed using the FEL. Unlike the measurements at $f = 29.5$ cm^{-1}, where the high-pass filter passed no detectable pump radiation, the measurements at 51.3 cm^{-1} were contaminated by leakage of the pump radiation.[23] It was also observed that the FEL produces its own second harmonics. Because of these contaminations to the bolometer signal, background subtraction is different from the case in which $f = 29.5$ cm^{-1}.

Figure 10 plots Fabry-Pérot scans with sample (a) depleted and (b) full. In Fig. 10(a) large peaks corresponding to the pump frequency occur spaced by $\lambda/2 = 97$ μm. In between each of these peaks small peaks occur, indicating the presence of a small SH component. We attribute this small SH mostly to the FEL, but it may also

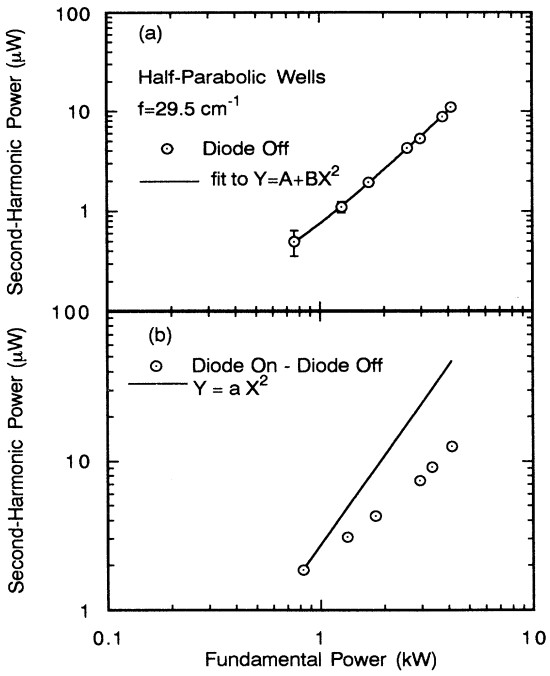

FIG. 9. Second-harmonic power vs fundamental power generated by the half-parabolic-well sample. (a) The second harmonic with diode off (circles) is well fit by a quadratic with an offset (solid line), consistent with the assignment as a signal generated by bulk GaAs. (b) The (second harmonic with diode on)−(fit to second harmonic with diode off) (circles) is not well fit by a quadratic (straight line), and is assigned to the confined electrons. The overall scale of the ordinate is uncertain by up to ±70% because of uncertainties in the collection efficiency of the second harmonic. The scale of the abscissa is uncertain by up to ±20%, and represents the power of the molecular gas laser averaged over the 60-ns width of the MGL pulse. Peak powers were larger, because of nanosecond time structure of the MGL pulse. Each point is the average of 50 pulses.

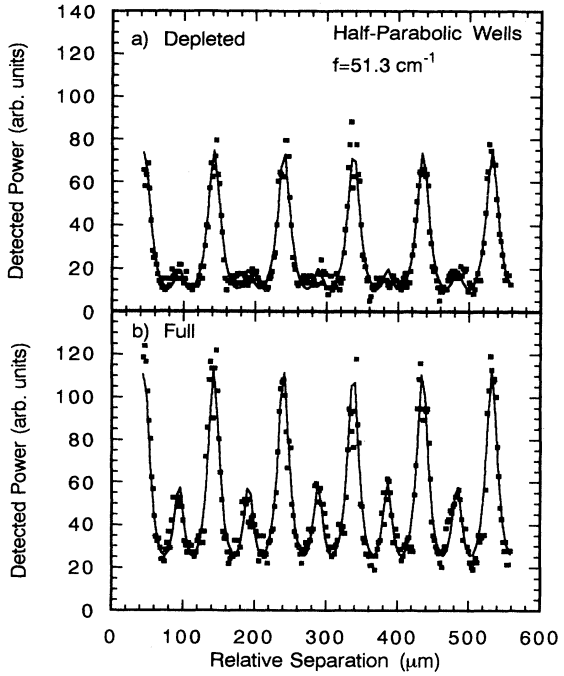

FIG. 10. Fabry-Pérot scan of the signal emitted by the half-parabolic-well sample in response to 51.3-cm^{-1} radiation from the UCSB FEL with the sample (a) depleted and (b) full. The large peaks in (a) are due to leakage of pump radiation through or around the waveguide filter. The smaller peaks, which are prominent in (b), indicate the presence of a second harmonic generated by the confined electrons. Energy per pulse $=2.5$ mJ, pulse length$=2.5$ μs, $T\approx 7$ K. The offset from zero is instrumental, and does not represent leakage through the FPI.

contain some small component from the bulk GaAs. The SH peaks in 10(b) are much more prominent than in 10(a), indicating a strong second harmonic generated by the confined electrons. The larger peaks spaced by $\lambda_{\text{pump}}/2$ are increased by approximately the same amount as the smaller peaks. Since the SH peaks are spaced by $\lambda_{\text{pump}}/4$, this is expected. This observation suggests that the primary effect of depleting the well of electrons is to quench second-harmonic emission, rather than change transmittance of the fundamental beam. The wavelength of the SH and pump beams was more precisely determined by measuring the FPI mesh separation, with sample full, for 100 small peaks and 50 large peaks, where we assumed that large peaks obscured small peaks. The results are shown in Table III, where the two wavelengths have been calculated and indicate the presence of a SH beam.

TABLE III. Wavelengths of the fundamental power and generated power for the free-electron laser line, showing that the generated power is the second harmonic of the fundamental. Wavelength = Separation/(2× Number of peaks).

Signal	Number of peaks	Separation (mm)	Wavelength (μm)
Small peaks	100	4.882±0.008	97.6±0.2
Large peaks	50	4.872±0.008	194.8±0.3

The intensity dependence of the emitted beam was measured with the sample depleted and full. The power detected by the bolometer with the sample depleted, P_B^{depl}, is plotted versus the fundamental power in the strip line, P_f, in Fig. 11. Each open circle is the average of 50 FIR pulses. The solid line is a *linear* fit with an offset of the form

$$P_{\text{fit}}^{\text{depl}} = C + D(P_f) \ . \tag{4}$$

The fit parameters are $C=-0.0756$ μW and $D=0.0396$. The success of the linear fit indicates that P_B^{depl} is predominantly due to leakage of the pump beam, and not to second harmonics generated by bulk GaAs.

The intensity dependence of the SH from the electrons in the well is exhibited in Fig. 11(b). We have extracted the SH emitted by the electrons by subtracting the fit (4) to the depleted signal from the full signal P_B^{full},

$$P_{2f}^{\text{electrons}} = P_B^{\text{full}} - P_{\text{fit}}^{\text{depl}}(P_f) \ . \tag{5}$$

$P_{\text{fit}}^{\text{depl}}$ was computed using the fitted parameters C and D. We see from Fig. 11(b) that the SH generated by the elec-

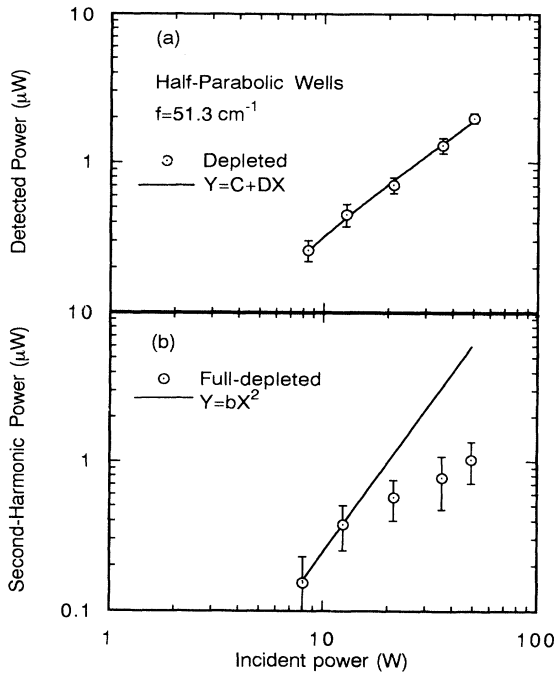

FIG. 11. (a) Detected power vs fundamental power for the sample depicted (circles) and fit to a *linear* power dependence with an offset (straight line). (b) Second-harmonic power (circles) = (detected power with sample full) − (detected power with sample depleted) vs fundamental power and quadratic fit (straight line). The second-harmonic signal in (b) is assigned to the confined electrons. The laser used here was the UCSB FEL. Since the UCSB FEL does not have the nanosecond time structure of the MGL, the scale of the abscissa more accurately reflects the peak power than does the scale on Figs. 9 and 14. Otherwise, uncertainties in the scales of the abscissa and ordinate are comparable to those for Fig. 9.

trons does not exhibit a quadratic dependence on the intensity of the fundamental, except perhaps at low power.

3. $f=27.7\ cm^{-1}$, molecular gas laser

A few measurements were also performed with fundamental $f=27.7\ cm^{-1}$. The second harmonic, at 55.4 cm^{-1}, was blocked by the waveguide cutoff filter. With this fundamental frequency, a small third-harmonic signal was observed, identified by a Fabry-Pérot scan. The signal was too small to be analyzed in detail.

D. Heterojunction sample

The following results are from the heterojunction sample at $T=7$ K with a pump frequency of 29.5 cm^{-1} from the MGL. The experimental protocol and data analysis are almost identical to those for the HPW sample at 29.5 cm^{-1}.

The frequency of the emitted beam was determined from measurements with the Fabry-Pérot interferometer to be the second harmonic, as in Fig. 7 for the HPW sample. In Fig. 12 the magnitudes of the bolometer signals produced by the second harmonic parallel and perpendicular to z are shown for the two cases diode on and diode off. Each measurement corresponds to an average of 50 FIR pulses. Figure 12 shows that, unlike for the 10-HPW sample, the horizontal component of the SH persists, although reduced, with the diode off. Figure 13 shows the components of the SH parallel and perpendicular to z with the diode on and the sample full and depleted by the application of a -713-mV bias to the gate. The application of the gate voltage nearly extinguishes the component parallel to z while the component perpendicular to z remains unaffected.

The intensity dependence of the SH was measured with sample depleted and full with the diode on. The second-harmonic power with sample full (depleted) will be denoted by $P_{2f}^{\rm full}$ ($P_{2f}^{\rm depl}$) and the fundamental power will be denoted by P_f. Figure 14(a) plots $P_{2f}^{\rm depl}$ vs P_f. Each point is the average of 50 FIR pulses. As for the HPW at 29.5 cm^{-1}, the solid curve is a fit to a quadratic pump intensity dependence with an offset of the form

$$P_{\rm fit}^{\rm depl}=E+F(P_f)^2 . \tag{6}$$

The fitted parameters are $E=0.121\ \mu$W and $F=0.895\ W^{-1}$. From the preceding results we conclude that the intensity of the second harmonic with the sample depleted depends quadratically on the intensity of the pump.

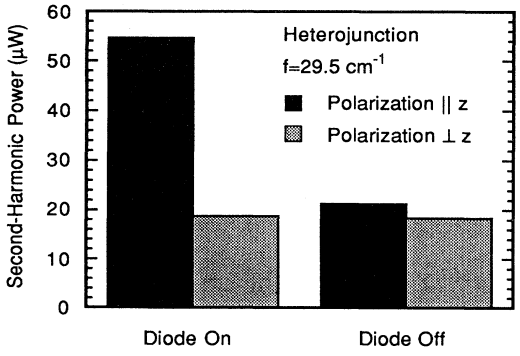

FIG. 12. Polarization content of the signal generated by the heterojunction sample with diode on and diode off. Unlike the half-parabolic-well sample, the polarization component parallel to z, which we attribute to the confined electrons, is only decreased by $\approx 60\%$ with diode off.

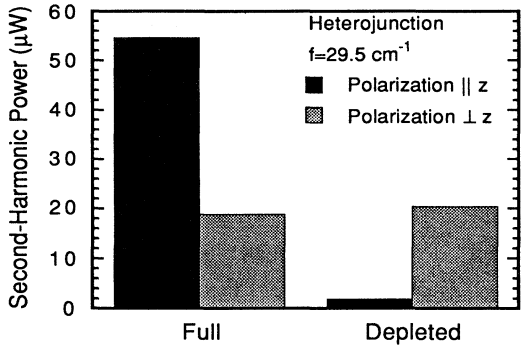

FIG. 13. Polarization content of the signal generated by the heterojunction sample with the sample full and depleted and application of a -713-mV gate bias. The polarization component parallel to z is decreased by 98% with the sample depleted.

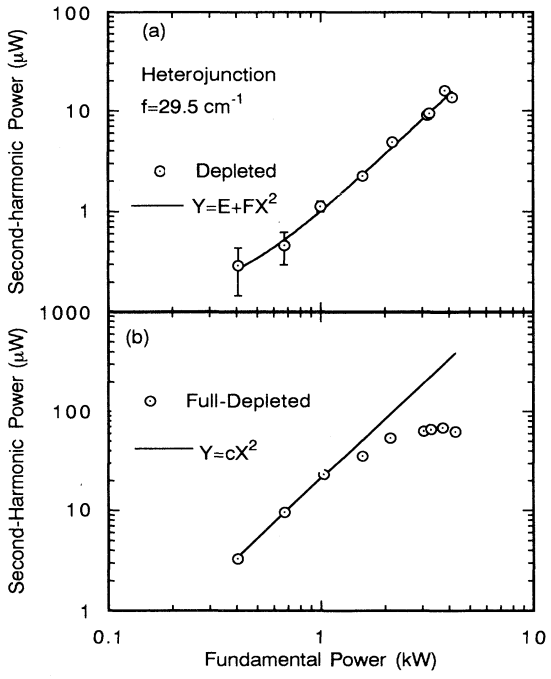

FIG. 14. Second-harmonic power vs fundamental power generated by the heterojunction sample. (a) The second harmonic with sample depleted (circles) is well fit by a quadratic with an offset (solid line) and is assigned to bulk GaAs. (b) The (second harmonic with sample full)$-$(fit to second harmonic with sample depleted) (circles) is well fit by a quadratic (straight line) at low powers, but not at high powers, and is assigned to the confined electrons. Uncertainties in the scales of the ordinate and abscissa are the same as for Fig. 9.

The intensity dependence of the component of the second harmonic parallel to z is shown in Fig. 14(b). We have extracted the component parallel to z by subtracting the fit (6) to the depleted signal from the full signal,

$$P_{2f}^{\text{electrons}} = P_B^{\text{full}} - P_{\text{fit}}^{\text{depl}}(P_f) \ . \tag{7}$$

$P_{2f}^{\text{electrons}}$ was computed using the fitted parameters E and F. Each point plotted is from the average of 50 FIR pulses. The three lowest points in Fig. 14(b) are consistent with a quadratic intensity dependence. At higher intensities, the second harmonic depends subquadratically on fundamental power—and even *decreases* at the highest intensity.

IV. ANALYSIS OF EXPERIMENTAL RESULTS

A. Calculation of surface second-order susceptibility from experimental results

Perturbation theory predicts that the generated second-harmonic power depends quadratically on the input fundamental power, with

$$P_{2f} \propto [\chi^{(2)} P_f]^2 \ , \tag{8}$$

where $\chi^{(2)}$ is independent of P_f and hence of the fundamental electric field amplitude E_f at the sample. The experimental results of Sec. III indicate a perturbative, quadratic regime at low powers for the heterojunction pumped with 29.5 cm^{-1}, but strongly subquadratic power dependences at higher powers for both samples. Strictly speaking, $\chi^{(2)}$ is not well defined where the intensity dependence is not quadratic. In the following we will parametrize the nonquadratic power dependence of the second harmonic by defining the surface second-order nonlinear susceptibility $\chi_S^{(2)}(E_f)$.[24]

Since a second-harmonic signal from bulk GaAs was observed for the data taken with the MGL, we can calculate $\chi_S^{(2)}$ relative to the value of $\chi^{(2)}$ for bulk GaAs for both samples. An advantage of a relative calculation is that it is not necessary to have absolute knowledge of the geometrical parameters or coupling efficiency of the pump beam, or of the collection efficiency of the SH. Furthermore, if $P_{2f} \propto P_f^2$, a relative calculation does not require absolute knowledge of the time structure of the pump beam, since the bulk and the electrons see the same time structure and it gets divided out. The inputs needed for a relative calculation of $\chi_S^{(2)}$ are the polarization content of the pump beam combined with the relative coupling efficiency of the two polarizations and $\chi^{(2)}$ for bulk GaAs (see the Appendix).

For a direct calculation of $\chi^{(2)}$, it is necessary to know the pump field amplitudes in the sample, and hence to know the pump beam parameters and the absolute coupling efficiency of the pump beam into the sample. It is also necessary to know the absolute collection efficiency of the second harmonic. The data taken with the FEL only allow for a direct calculation of $\chi_S^{(2)}$ for the HPW sample—the peak power of the FEL was insufficient to observe a bulk signal.

The following data were used in the calculation of the pump field amplitude in the sample, and relative and direct values of $\chi^{(2)}$. The pump beam from the MGL was determined to be polarized at $\theta = (3.8 \pm 1.0)°$ above horizontal or z direction. As mentioned in the Appendix, the two polarizations of the free-space pump beam couple to their respective waveguide modes inside the strip line with the same efficiency. The pump beam is assumed to uniformly fill the sample in the x direction along its width $w \approx 0.5$ cm. From the linear transmission of the strip line coupler containing the 10-HPW sample at $T = 7$ K, the absolute coupling efficiency of the pump beam polarized (parallel, perpendicular) to z was determined to be $[(4.7 \pm 0.3)\%, (8.9 \pm 0.7)\%]$. The transmitted signal did not depend on the electron density in the sample, indicating negligible intersubband absorption. The length of the MGL FIR pulse is approximately $\tau_L \approx 60$ ns with an energy per pulse at 29.5 cm^{-1} measured to be $E_p = 5 \pm 2$ mJ. The collection efficiency of the SH was determined experimentally to be $\alpha = 0.03 \pm 0.02$. The length contraction of the samples upon cooling to $T = 7$ K was determined from Ref. 25 to be $\Delta l / l = -1.267 \times 10^{-3}$. The value of $\chi^{(2)}$ for bulk GaAs was measured by Mayer and Keilmann[19] at $T = 300$ K to be $\chi^{(2)} = (1.3 \times 10^{-7} \pm 0.8 \times 10^{-7})$ $\text{cm}^{-2}\,\text{esu}^{-1}$ for a pump frequency of 29.5 cm^{-1}.

The result of the relative calculation of $\chi_S^{(2)}$ for the heterojunction pumped by the MGL at 29.5 cm^{-1} is shown in Fig. 15(a) plotted versus the rms fundamental

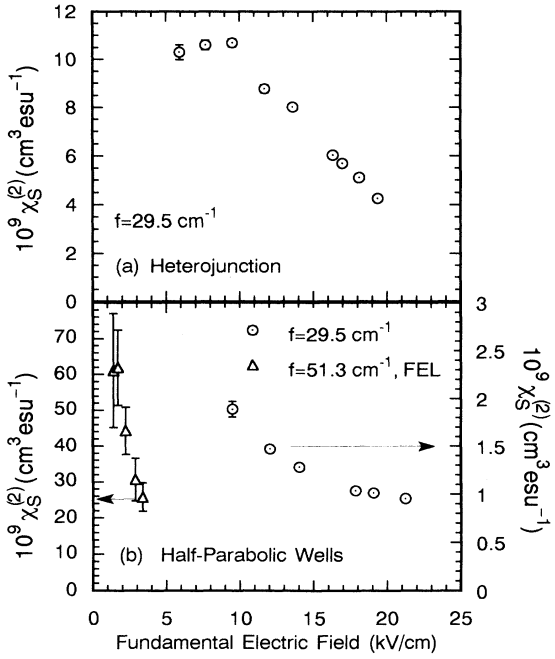

FIG. 15. Surface second-order nonlinear susceptibility $\chi_S^{(2)}$ vs fundamental electric field for (a) the heterojunction at $f = 29.5$ cm^{-1} (relative calculation, see text), (b) the half-parabolic wells at $f = 29.5$ cm^{-1} (relative calculation) and at $f = 51.3$ cm^{-1} (direct calculation). The radiation sources for the 29.5- and 51.3-cm^{-1} radiation were the molecular gas laser and the UCSB FEL, respectively. The fundamental electric fields used to plot this graph were averaged over the 60-ns width of the MGL pulse. Because of intrapulse fluctuations on the MGL, peak fields were higher.

electric field at the heterojunction (which is entirely polarized parallel to z because of the boundary condition set by the gold gate). The rms fundamental field amplitude is calculated by using the pulse length and energy given previously. Instantaneous fields may be several times larger than shown due to the nanosecond intrapulse time structure of the MGL FIR pulses. The heterojunction $\chi_S^{(2)}$ is approximately constant at rms fundamental electric field strengths below 10 kV/cm, and then begins to drop approximately linearly with electric-field amplitude. Because of uncertainties in experimental parameters, the overall scales of the abscissa ($\chi_S^{(2)}$) and ordinate (fundamental electric field) are uncertain by ± 0.75 and ± 0.25, respectively. The error bars represent the magnitude of the standard errors due to pulse-to-pulse fluctuations in the lasers and measurement noise. For fundamental electric fields below 10 kV/cm, $\chi_S^{(2)} = 1 \pm 0.75 \times 10^{-8}$ $\text{cm}^{-2}\,\text{esu}^{-1}$.

Figure 15(b) shows a relative calculation of $\chi_S^{(2)}$ versus fundamental electric field for the HPW sample at $f = 29.5\ \text{cm}^{-1}$. At 29.5 cm^{-1}, even for the smallest measured fundamental electric fields, $\chi_S^{(2)}$ for the HPW decreases with increasing fundamental electric field. The magnitude of $\chi_S^{(2)}$ for the HPW is smaller at 29.5 cm^{-1} than for the heterojunction sample.

Direct calculations of $\chi^{(2)}$ for bulk GaAs and $\chi_S^{(2)}$ were also performed. From second-harmonic data with the depleted heterojunction and the HPW sample with diode off, $\chi^{(2)}$ of bulk GaAs at 29.5 cm^{-1} were found to be 7.5×10^{-8} $\text{esu}^{-1}\,\text{cm}^2$ and 9×10^{-8} $\text{esu}^{-1}\,\text{cm}^2$ with an uncertainty $\Delta\chi^{(2)}/\chi^{(2)} = 0.75$. These are within experimental error of the values quoted by Mayer *et al.*, 1.3×10^{-7} $\text{esu}^{-1}\,\text{cm}^2$, with an uncertainty $\Delta\chi^{(2)}/\chi^{(2)} = 0.5$. By construction, calculated values of $\chi_{S\,\text{Direct}}^{(2)}$ differ from $\chi_{S\,\text{Relative}}^{(2)}$ by only a scale factor $s = \chi_{S\,\text{Direct}}^{(2)}/\chi_{S\,\text{Relative}}^{(2)}$. This factor $s = 0.6$, and thus direct and relative values of $\chi_S^{(2)}$ are within experimental error of one another and our analysis is internally consistent.

Figure 15(b) also shows a direct calculation of $\chi_S^{(2)}$ for the HPW using the FEL at 51.3 cm^{-1}. Again, the magnitude of $\chi^{(2)}$ decreases with increasing rms pump field amplitude. The error in this calculation is $\Delta\chi_S^{(2)}/\chi_S^{(2)} = \pm 0.47$. The values of $\chi_S^{(2)}$ for the HPW at 51.3 cm^{-1} are significantly larger than at 29.5 cm^{-1}, indicating the possibility of a resonant enhancement. However, experiments must be repeated at many frequencies on better-characterized samples before making much of such an enhancement.

B. Comparison with other measurements on quantum wells and bulk GaAs

We now compare our measured values of the second-order susceptibility for a heterojunction at 330-μm wavelength with previously measured values for dc-biased square wells and square wells with a "step" in Al concentration on one side. For purposes of comparison, we choose only our low-intensity values of $\chi^{(2)}$, where $\chi^{(2)}$ is independent of FIR field strength. We have converted the bulk susceptibilities in Refs. 3 and 4 to surface susceptibilities per well by simply multiplying the published values by the width of the wells, ≈ 100 Å in each case.

TABLE IV. Surface nonlinear susceptibilities for different quantum wells.

Sample	Wavelength (μm)	$\chi_S^{(2)}$ per well ($\text{cm}^3\,\text{esu}^{-1}$)	Resonant
Heterojunction (this work)	330	$1.0 \pm 0.75 \times 10^{-8}$	no
Step well[a]	10.6	1.7×10^{-9}	yes
Biased square well[b]	10.6	6.7×10^{-11}	yes

[a]Reference 4.
[b]Reference 3.

In each case, the charge density per well was approximately 5×10^{-11} cm^{-2}. Even though the FIR measurements on the heterojunction were far from a resonance and the mid-infrared measurements on the step well were on a double resonance, the FIR $\chi_S^{(2)}$ for the heterojunction is one order of magnitude larger.[16] (See Table IV.)

The nonlinear polarizability of an electron in our heterojunction at $f = 29.5$ cm^{-1} can be calculated: $\alpha^{(2)} = \chi_S^{(2)}/N_S = 2 \times 10^{-20}$ $\text{cm}^5\,\text{esu}^{-1}$. This is approximately nine orders of magnitude larger than the nonlinear polarizability of a valence electron at the same frequency, calculated using the bulk $\chi^{(2)} = 10^{-7}$ $\text{esu}^{-1}\,\text{cm}^2$ measured by Mayer and Keilmann[19] and assuming a density of 10^{22} valence electrons/cm^3.

V. COMPARISON OF EXPERIMENTAL RESULTS WITH THEORY

A. Simple perturbative theory

Comparison of our experimental result with a theoretical calculation of $\chi_S^{(2)}$ is possible where there is a quadratic dependence of $I_{2\omega}$ on I_ω, i.e., at low intensities in the heterojunction sample for $f = 29.5$ cm^{-1}. We begin this section with a brief description of the physics of the heterojunction, then calculate $\chi_S^{(2)}$ in the simplest approximation, and finally compare the calculation with our experimental results.

The wave functions and energy levels of electrons confined at a GaAs/$\text{Al}_x\text{Ga}_{1-x}$As heterojunction may be approximated by those of an electron in a triangular potential

$$V(z) = \infty\ ,\quad z < 0\ , \tag{9a}$$

$$V(z) = eFz\ ,\quad z > 0\ , \tag{9b}$$

as in Ref. 12, where F is a built-in electric field. F is determined primarily by charge transfer from the donors in the $\text{Al}_x\text{Ga}_{1-x}$As barrier to the GaAs, but is also affected by unintentional p-type doping in the $\text{Al}_x\text{Ga}_{1-x}$As. The solutions are Airy functions with the eigenvalues given asymptotically for large n as

$$E_n \approx \left[\frac{\hbar^2}{2m^*}\right]^{1/3}\left[\frac{3\pi eF}{2}(n+\tfrac{3}{4})\right]^{2/3}, \quad n=0,1,2\ldots . \tag{10}$$

For $n=0,1,2$ the exact eigenvalues have $n+\frac{3}{4}=0.7587$, 1.7540, and 2.7575, respectively. For an areal density of $N_s=5\times10^{11}$ cm^{-2} and an acceptor density of $N_{ac}=10^{15}$ cm^{-3} the ground-state energy is taken from self-consistent calculations by Stern *et al.* to be $E_0=49$ meV.[12] With the above value for E_0, eF in Eq. (10) is found to be $eF=39$ kV/cm. The transition between ground and first-excited states occurs at 290 cm$^{-1}=36$ meV/$\hbar$, which is much larger than our pump frequency $f=29.5$ cm^{-1}.

An expression for the second-order polarizability of an electron confined to discrete states is given in Ref. 10 as

$$\alpha_{33}^{(2)}=\frac{2e^3}{\hbar^2}\sum_{mn}\langle z_{1n}\rangle\langle z_{nm}\rangle\langle z_{m1}\rangle \times\{[(\omega-\omega_{n1})(2\omega-\omega_{m1})]^{-1}+[(\omega+\omega_{n1})(2\omega+\omega_{m1})]^{-1}-(2\omega-\omega_{mn})^{-1}[(\omega-\omega_{m1})^{-1}+(\omega+\omega_{n1})^{-1}]\} \tag{11}$$

where the sum is over all i and j, $\langle z_{ij}\rangle$ are the dipole transition matrix elements, and $\omega_{ij}=(E_i-E_j)/\hbar$ where E_i and E_j are intersubband energy levels. The surface susceptibility is simply

$$\chi_S^{(2)}=N_S\alpha^{(2)} . \tag{12}$$

The approximations behind (11) are the following.

(1) The system is in its ground state before the perturbation is turned on. This is reasonable since at $T=7$ K, where the experiments were carried out, $E_{21}=36$ meV $\gg k_BT=0.6$ meV.

(2) The ground state has no permanent dipole moment.[27] This assumption implies $\langle z_{11}\rangle=0$, which sets the origin for the calculation of all dipole matrix elements. Without this assumption, Eq. (11) diverges at zero frequency.

(3) The pump frequency $\omega=2\pi f$ is far from any resonance, and thus intersubband lifetimes can be set to infinity. This is reasonable since $f=29.5$ cm^{-1} is ten times smaller than the lowest intersubband transition.

(4) Electron-electron interactions are not fully treated. The Coulomb interaction is taken into account to a certain extent in determining the slope eF of the triangle well, but Eq. (11) is certainly not a full-blown self-consistent calculation of $\chi_S^{(2)}$. We are aware of no such calculations for electrons in quantum wells.

(5) The electrons remain primarily in their ground state throughout the length of the pulse. The quadratic dependence of $I_{2\omega}$ on I_ω at low intensities indicates that this is largely true for these intensities.

The assumption behind (12) is the following.

(6) The polarizations induced in the 2D electrons do not significantly affect the local fields. We have shown elsewhere that this is true for our experiments.[28]

The intersubband level spacings and dipole transition matrix elements were calculated numerically for a triangular well that is 225-meV deep with a slope of $eF=39$ kV/cm and inserted in Eqs. (11) and (12) along with $N_S=5\times10^{11}$ cm^{-2} to calculate $\chi_S^{(2)}$. The calculated value of $\chi_S^{(2)}$ for the heterojunction is 8.3×10^{-9} cm^{3}esu^{-1} (3.48×10^{-12} m^2/V). This is within experimental error of the measured value of $(1.0\pm0.75)\times10^{-8}$ cm^{3}esu^{-1} ($4\pm3\times10^{-12}$) m^2/V.

The calculated value for the heterojunction is dominated by the term with $i=j=2$—a two-level approximation. In fact, the zero-frequency, two-level approximation

$$\chi_S^{(2)}=\frac{N_Se^3}{\hbar^2}\frac{8\langle z_{12}\rangle\langle z_{22}\rangle\langle z_{21}\rangle}{(\Omega_{12})^2} \tag{13}$$

gives 1.0×10^{-8} cm^{3}esu^{-1}, within 20% of the value obtained from evaluating the full sum (11) for $\omega/2\pi=30$ cm^{-1}. For comparison, the surface susceptibility on a double resonance ($\omega=\Omega_{12}$ and $2\omega=\Omega_{13}$—as in the step well studied in Ref. 4 by Boucaud *et al.*) can be approximated by

$$\chi_S^{(2)}=\frac{N_Se^3}{\hbar^2}\frac{2\langle z_{12}\rangle\langle z_{23}\rangle\langle z_{31}\rangle}{(\gamma)^2} , \tag{14}$$

where $\gamma=\gamma_{12}=\gamma_{13}$ is a relaxation rate assumed to be the same for the two transitions involved.[29] The enhancement of $\chi_S^{(2)}$ for the heterojunction at 330 μm over the step well at 10 μm is primarily because of the larger matrix elements.

The values of $\chi^{(2)}$ at 29.5 cm^{-1} for the half-parabolic-well sample, if the potentials really were as designed to have a transition between the ground and first-excited states at 50 cm^{-1}, should have been more than one order of magnitude larger than for the heterojunction. However, as stated above, capacitance-voltage profiling shows that almost all of the charge in the HPW's was concentrated in the first two wells. In this case, band bending similar to what occurs in a heterojunction would effectively add a strong linear term eFz to the half-parabolic potential, and the potential seen by the electrons in the HPW's would have been similar to the triangular potential of a heterojunction, with intersubband transitions pushed up to over 200 cm^{-1}. Transmission spectra showed no evidence of intersubband absorptions in the HPW's between 40 and 200 cm^{-1}, consistent with this scenario. With more careful band-gap engineering in a HPW to cancel out the linear terms in the potential, much larger values of $\chi^{(2)}$ than those observed here should be achievable.

B. Nonperturbative effects

Saturation of second-harmonic generation in GaAs-$Al_xGa_{1-x}As$ asymmetric quantum wells was first reported by Boucaud *et al.*[30] for pump wavelengths near 10 μm. The sample they used was the step well tuned to a double resonance, which was discussed above and in Ref. 4. They observed a dependence of the second-harmonic power on fundamental power similar to that which we observe for the heterojunction [Fig. 14(b)]—quadratic at low intensity and subquadratic at high intensity. The saturation of second-harmonic efficiency is related to population saturation in their paper: "The saturation of the SHG efficiency and that of the first intersubband transition occur at approximately the same pump intensity." The intensities used by Boucaud *et al.* were sufficient to create a highly nonequilibrium distribution of electrons among the unperturbed energy levels of the system, but not sufficient to significantly shift those levels through what they call dynamic Stark effects.

In the mid-infrared, resonant three-photon ionization from a quantum well has been observed by Sirtori *et al.*[31] The sample contained an $Al_xIn_{1-x}As/Ga_xIn_{1-x}As$ quantum well in which three photons with energy ≈ 100 meV ($\lambda \approx 10$ μm) could, via two resonant intermediate states, couple the ground state to the continuum.

Our excitation frequency in the heterojunction samples was ≈ 10 times smaller than any intersubband resonance. Thus it is unlikely that the saturation mechanism deduced by Boucaud *et al.* explains our nonperturbative results. The FIR electric fields of up to 20 kV/cm are comparable to the 39 kV/cm estimated above to be confining the electrons at the heterojunction. At these large FIR electric fields, dynamic Stark effects cannot be ignored. The ionization we observe is also not a resonant process, and thus quite different from that observed by Sirtori *et al.* Approximately 65 photons (=240 meV/3.7 meV) are required to ionize an electron from the ground state of the wells we studied here. Naively, this would imply the need to go to 65th order in a perturbative treatment. A completely nonperturbative treatment is necessary to explain our results, which takes into account both dynamic Stark shifts and ionization during the course of the pulse.

VI. CONCLUSION

We have demonstrated FIR harmonic generation from semiconductor heterostructures. We observed nonresonant values of surface susceptibility $\chi_S^{(2)}$ which are comparable to resonant values achieved near 10 μm. The $\chi_S^{(2)}$ measured for a heterojunction at low intensities agrees within experimental error with that calculated from a simple model. It would be interesting to see a more sophisticated calculation which includes electron-electron interaction in a self-consistent fashion. At the highest intensities used, the intensity of the second harmonic depends subquadratically on the intensity of the fundamental, and electrons are ionized from the quantum wells by the FIR pulses. These observations signal a breakdown of perturbation theory and indicate a strong need for new theoretical analysis.

At the highest intensities, we are in a regime similar to that achieved in experiments on atoms in intense laser fields. In the experiments on atoms, laser fields comparable to the Coulomb binding field are applied. Observed phenomena include the generation of harmonics of very high order.[32] It is an exciting possibility that similar phenomena can be observed in quantum wells under intense FIR radiation, which may be thought of as "solid-state atoms."

ACKNOWLEDGMENTS

We thank S. J. Allen, J. Beeman, B. Birnir, K. Ensslin, B. Galdrikian, R. Grauer, E. Gwinn, E. E. Haller, M. Holthaus, D. Lang, A. Markelz, R. Prange, R. Scharf, B. Sundaram, and A. Wixforth for extremely helpful and stimulating discussions. We thank E. E. Haller and J. Beeman for assistance with FIR detection. This work was supported by NSF-DMR 8901651, ARO-YIP 29185 and the Alfred P. Sloan Foundation (M.S.S), AFOSR 88-0099 and AFOSR 91-0214 (A.C.G, M.S., and P.F.H.), SDIO-ONR N00014-K-0110V and ONR N0014-92-J-1452 (W.W.B., C.L.F., and J.J.P.), and the NSF Science and Technology Center for Quantized Electronic Structures, Grant Nos. DMR-88-10430 and DMR-91-0214 (clean room access).

APPENDIX: ANALYSIS OF THE STRIP LINE COUPLER

The strip line coupler used in the experiments is shown schematically in Fig. 16, with sample and entrance width labeled *a* and *d*, respectively. The purpose of the strip line coupler is to couple free-space electromagnetic (EM) fields to waveguide modes in the sample. The coupler consists of two thin, curved beryllium copper leaves that are ~1-cm high and ~4-in. long. The sample is sandwiched between the leaves and one of the leaves is cut away in the sample region to allow illumination with an IR LED. The input and output ends of the leaves

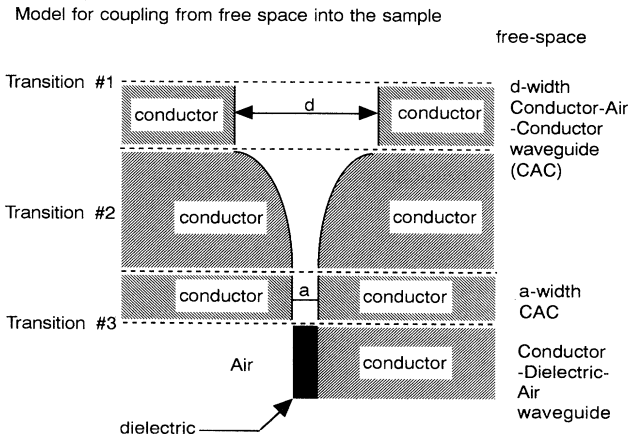

FIG. 16. Schematic diagram of the horn and strip line, as broken down for purposes of analysis.

consist of copper apertures that are ~ 1 cm in diameter. Presented here is a brief outline of an analysis too lengthy to present in detail.[28]

The coordinates used in our analysis are defined in Fig. 5. The z direction is the growth direction for the sample, which has a width $a = 0.05$ cm. The radiation propagates in the x direction. For the purpose of analysis, the strip line is modeled as infinite in the y direction. All the metal surfaces are considered to be perfect conductors which are infinite in the y direction. For the analysis the coupler is divided into four distinct regions connected by three transitions, as shown in Fig. 16. The input and output of the strip line coupler are considered to be symmetric. As the strip line is traversed in the x direction, the regions encountered are free space; a conductor-air-conductor (CAC) waveguide with air gap width $d \sim 1$ cm to model the aperture before the Be-Cu leaves; a CAC waveguide with air gap width $a = 0.05$ cm to model the entrance to the sample; and a conductor-dielectric-air (CDA) waveguide with dielectric width $a = 0.05$ cm and length l to model the sample with metal on one side and free space on the other. The first transition is between free space and the d-width CAC waveguide. The second transition is the tapered section of the CAC waveguide and couples the d-width CAC guide to the a-width CAC guide. The third transition is between the a-width CAC guide and the CDA guide.

For the calculations regarding linear propagation in the CDA waveguide, the sample is treated as a uniform dielectric with the constants of bulk GaAs. The contribution to the dielectric constant of the heterostructure is neglected because it was calculated to be less than one percent of the bulk constants.[28]

With the previous assumptions the analysis begins by deriving the form of the modes for the CAC and CDA waveguides. Both waveguides have two distinct types of modes that are characterized by their polarization content. The transverse-magnetic (TM_n) modes have horizontal ($\|z$) and longitudinal ($\|x$) components of electric field and the transverse-electric (TE_n) modes have only a vertical ($\perp z$) component of electric field. The modes for the two waveguides differ in their spatial dependence in the horizontal direction (i.e., growth direction of the sample) and propagation constants in the longitudinal direction. The CAC waveguide has a TEM or TM_0 mode while the CDA waveguide does not. Expressions for the transmission and reflection at the a-width CAC-to-CDA waveguide transition are derived in a variational approximation.[33] The transition from the free-space region to the d-width CAC guide and the tapered transition are analyzed in the variational approximation combined with the above analysis of the waveguide modes. We deduce that the horizontal and vertical components of the free-space electric fields couple effectively to only the lowest order or TM_1 and TE_1 CDA waveguide modes, respectively. The results of the linear transmission measurements for the respective polarizations were analyzed in the above approximation and indicate that the horizontal and vertical components of the free-space fields couple to the a-width CAC TM_0 and TE_1 modes with equal efficiency.

Second-harmonic generation in the CDA waveguide that is the sample is analyzed as a traveling waveguide process, as described in Ref. 34. For the analysis the heterostructure is considered to be two dimensional and located at the conductor-dielectric interface of the CDA waveguide thus giving rise to a surface polarization at the interface with an associated second-order surface susceptibility $\chi_S^{(2)}$. The growth of the sample and the strip line coupler geometry determine that the TM_1 CDA pump mode will generate SH's from the heterostructure that will couple to the TM_1 CDA mode at the SH and radiate to free space with a horizontal polarization ($\|z$). The symmetry class of GaAs and the coupling geometry determine that the TM_1 and TE_1 CDA pump modes will interact to generate SH's from bulk GaAs that will couple to the TE_1 CDA mode at the SH and radiate to free space with a vertical polarization ($\perp z$). The above modeling allows us to calculate $\chi_S^{(2)}$ for the heterostructure relative to $\chi^{(2)}$ for bulk GaAs when both the second harmonics are measurable.

[1] C. Weisbuch and B. Vinter, *Quantum Semiconductor Structures* (Academic, Boston, 1991).

[2] M. K. Gurnick and T. A. DeTemple, IEEE J. Quantum Electron. **QE-19**, 791 (1983).

[3] M. M. Fejer, S. J. B. Yoo, R. L. Byer, A. Harwit, and J. S. Harris, Jr., Phys. Rev. Lett. **62**, 1041 (1989).

[4] P. Boucaud, F. H. Julien, D. D. Yang, J.-M. Lourtioz, E. Rosencher, P. Bois, and J. Nagle, Appl. Phys. Lett. **57**, 215 (1990).

[5] P. Boucaud and F. H. Julien, J. Phys. (France) III **1**, 13 (1991).

[6] P. Bois, E. Rosencher, J. Nagle, E. Martinet, P. Boucaud, F. H. Julien, D. D. Yang, and J.-M. Lourtioz, Superlatt. Microstruct. **8**, 369 (1990).

[7] S. J. B. Yoo, M. M. Fejer, R. L. Byer, and J. S. Harris, Jr., Appl. Phys. Lett. **58**, 1724 (1991).

[8] C. Sirtori, F. Capasso, D. L. Sivco, and A. Y. Cho, Phys. Rev. Lett. **68**, 1010 (1992).

[9] J. F. Ward, Rev. Mod. Phys. **37**, 1 (1965).

[10] Y. R. Shen, *The Principles of Nonlinear Optics* (Wiley, New York, 1984).

[11] M. Sundaram, S. A. Chalmers, P. F. Hopkins, and A. C. Gossard, Science **254**, 1326 (1991).

[12] F. Stern and S. Das Sarma, Phys. Rev. B **30**, 840 (1984).

[13] See, for example, *Atoms in Intense Laser Fields,* edited by M. Gavrila (Academic, Boston, 1992).

[14] M. S. Sherwin, in *Quantum Chaos,* edited by G. Casati and B. V. Chirikov (Cambridge University Press, Cambridge, England, in press).

[15] See, for example, A. C. Gossard, IEEE J. Quantum Electron. **QE-22**, 1649 (1986); M. Sundaram, S. A. Chalmers, P. F. Hopkins, and A. C. Gossard, Science **254**, 1326 (1991).

[16] A computer program written by Dr. Greg Snider was used for this calculation.

[17] For a review of the physics of deep donors in III-V compounds, see P. M. Mooney, J. Appl. Phys. **67**, R1 (1990).

[18] C. T. Gross, J. Kiess, A. Mayer, and F. Keilmann, IEEE J. Quantum Electron. **QE-23**, 377 (1987).

[19] A. Mayer and F. Keilmann, Phys. Rev. B **33**, 6954 (1986).

[20]F. Keilmann, Int. J. Infrared Millimeter Waves **2**, 259 (1981).

[21]J. J. Plombon, W. W. Bewley, C. L. Felix, M. S. Sherwin, P. Hopkins, M. Sundaram, and A. C. Gossard, Appl. Phys. Lett. **60**, 1972 (1992).

[22]In this paper, the second-harmonic power emitted by the sample was extracted from the bolometer signal as follows: A boxcar integrator detected the peak of the voltage pulse generated by the radiation hitting the bolometer. This voltage V was converted to $P=V/S\eta(\tau_B/\tau_L)$, where $S=2.57\times10^5$ V/W is the responsivity of the bolometer, $\eta\approx0.03\pm0.02$ is the collection efficiency for the second-harmonic radiation, $\tau_B=200$ μs is the time constant of the bolometer, and $\tau_L=60$ ns (2.5 μs) is the width of the FIR pulse from the MGL (FEL). Because of the large uncertainty in collection efficiency, the absolute magnitude of the second-harmonic power is uncertain by up to a factor of 5. The maximum (unattenuated) fundamental power in the strip line $P_f=U\eta_s/\tau_L$, where U is the FIR energy per pulse (≈5 mJ for the MGL, 2.5 mJ for the FEL), $\eta_s=0.05$ is the transmittance of the strip line with a cold sample, and τ_L is the pulse width of the FIR laser. Because of large intrapulse fluctuations, peak powers with the MGL were higher than the average over 60 ns quoted here. Attenuated fundamental power was proportional to the signal on reference detector no. 2 (Fig. 4).

[23]Subsequent to these measurements, we discovered that the filter mount had developed light leaks. We are unsure whether the leakage at 51.3 cm^{-1} came through or around the filter, but, given our experimental protocol, it does not matter.

[24]For an outline of how E_f was calculated from experimental measurements, see the Appendix.

[25]J. S. Blakemore, J. Appl. Phys. **53**, R123 (1982).

[26]For the scientific purposes of this paper, it is useful to compare surface nonlinear susceptibilities. For technological purposes, one needs also to consider how closely one can pack asymmetric two-dimensional (2D) electron layers to achieve a large nonlinear susceptibility per unit volume. The step wells can be made in a superlattice with a period of approximately 200 Å, while a superlattice of heterojunctions needs to have a period roughly an order of magnitude larger. Thus the nonlinear susceptibility per unit volume in a superlattice of heterojunctions like the one measured here at 330 μm would be of the same order of magnitude (a few $\times10^{-7}$ m/V) as a superlattice of step wells, like those in Ref. 4, at 10 μm.

[27]Y. R. Shen, *The Principles of Nonlinear Optics* (Ref. 10), p. 16.

[28]W. W. Bewley, Ph.D. thesis, University of California–Santa Barbara, 1992.

[29]E. Rosenscher, P. Bois, J. Nagle, and S. Delaitre, Electron. Lett. **25**, 1063 (1989). Note that Eq. (14) differs by a factor of 2 from Eq. (3) of Rosenscher *et al.*

[30]P. Boucaud, F. H. Julien, D. D. Yang, J.-M. Lourtioz, E. Rosenscher, and P. Bois, Opt. Lett. **16**, 199 (1991).

[31]C. Sirtori, F. Capasso, D. L. Sivco, and A. Y. Cho, Appl. Phys. Lett. **60**, 2678 (1992).

[32]See, for example, A. L'Huillier, L.-A. Lompré, G. Mainfray, and C. Manus, in *Atoms in Intense Laser Fields* (Ref. 13), p. 139.

[33]R. A. Waldron, *Theory of Guided Electromagnetic Waves* (Van Nostrand Reinhold, London, 1969), p. 483.

[34]Y. R. Shen, *The Principles of Nonlinear Optics* (Ref. 10), pp. 505–509.